Investigation of Electron-phonon Interaction Phenomena in the LaF_3–Nd^{3+} Crystal

D. N. VYLEGZHANIN AND A. A. KAMINSKIĬ

Crystallography Institute, USSR Academy of Sciences

Submitted July 23, 1971

Zh. Eksp. Teor. Fiz. **62**, 685–700 (February, 1972)

The shift and broadening of phononless lines in the LaF_3–Nd^{3+} crystal are studied by the stimulated emission spectroscopy technique in a broad temperature range. Resonance and Raman scattering of phonons were taken into account in the interpretation of the results. The energy characteristics of the laser are investigated and information is obtained regarding the temperature dependence of the probability for the nonradiative transition $^4I_{11/2}$–$^4I_{9/2}$. It is found that the variation of the probability with temperature can be ascribed to a relaxation process involving the emission of five phonons with energies ~ 300 cm^{-1}. The spectral composition of the stimulated radiation at 77–820°K is studied in detail. Generation is recorded for seven transitions between the terms $^4F_{3/2}$ and $^4I_{11/2}$. Dependences of the generation threshold energy are obtained for LaF_3–Nd^{3+} crystals with various orientations of the optical axis and an interpretation of the results is presented.

INTRODUCTION

THE interaction of impurity ions with lattice vibrations causes a temperature shift of the spectral lines and their broadening, nonradiative transitions (NT), and the appearance of electron-vibrational satellites in the optical spectra. All these manifestations of the electron-phonon interaction are now being extensively investigated by the usual spectroscopic methods. Recent investigations[1] indicate that the methods of stimulated emission (SE) spectroscopy also make it possible to obtain valuable and in some cases even more complete information concerning this phenomenon. An important fact is that in the SE regime it is possible to reach temperatures at which traditional luminescence and absorption analyses result in large errors or cannot be used at all as a result of the broadening and coalescence of the lines. Unfortunately, such investigations can be carried out in a wide temperature interval only with media activated with Nd^{3+} ions. Our purposes were to carry out a comprehensive investigation of the manifestations of electron-phonon interaction by studying the SE parameters in LiF_3 crystals activated with Nd^{3+} ions, and also to obtain more complete information on the spectral composition of the SE and to measure a number of spectral characteristics necessary for a theoretical analysis of the operation of a laser based on this crystal.

CRYSTALS, APPARATUS, AND INVESTIGATION PROCEDURES

We used in the experiments LaF_3 single crystals with activator concentrations from 0.5 to ~2 wt.% (NdF_3/LaF_3 in the charge) and with different optical-axis orientations. These were used to prepare "active elements" in the form of cylindrical rods of length from 7 to ~30 mm and of diameter ~5 mm with plane-parallel end faces (~15″). The angle ζ between the optical axis c and the geometrical axis F of the crystals was determined by x-ray diffraction accurate to ~3%. In experiments with lasers with combined active media (CAM)[2], we used also mixed fluoride crystals α-$NaCaYF_6:Nd^{3+}$ and α-$NaCaCeF_6:Nd^{3+}$, and type LGS-41K neodymium glass. The loss in $LaF_3:Nd^{3+}$ was approximately 0.03 cm^{-1}. The spectroscopic properties of $LaF_3:Nd^{3+}$ were investigated by standard methods. The lasing characteristics of $LaF_3:Nd^{3+}$ were investigated by SE-spectroscopy methods developed in our laboratory[1].

We used several illuminating systems in the experiments. At low temperatures (to 300°K) we used a chamber of elliptical cross section with a xenon lamp of the IFP-400 type. At 77°K, the investigated samples, located in a tubular glass cryostat, were in direct contact with the liquid nitrogen. This system also made it possible to obtain intermediate temperatures, which were monitored with a copper-constantan thermocouple fixed to the crystal and with an F-116/2 microvoltmeter. In this case the coupling between the active element and the optical resonator was effected with the aid of special quartz light pipes. The measurements at $T > 300$°K were performed with the illuminators described in detail in[3]. In an earlier analysis[3] of SE of a number of crystals with Nd^{3+} ions it was observed that the high-temperature lasing limit depends significantly on the spectral composition of the exciting radiation. To obtain the most reliable information on the SE parameters we surrounded the pump lamps in our experiments with a filter made of ZhS-17 glass. At the high temperature investigations, to prevent changes in spectral parameters of the lamp and in the filter by heat, the latter were water-cooled.[4]

To excite the additional $LaF_3:Nd^{3+}$ generation lines, for the purpose of studying their temperature dependence, an SE spectroscopy method using a laser with CAM was used[2,5]. In this case the optical resonator contained, in addition to the investigated crystal, also a second medium excited by its own autonomous pump system. In such experiments, the combining media could have different temperatures. The SE spectra were investigated photographically (I-1070) with a DFS-8-spectrograph (~5.9 Å/mm, 600 lines/mm).

EXPERIMENTAL RESULTS

The investigation of the thermal shift of the Nd^{3+}-ion levels in LaF_3 crystals was initiated by Johnson

et al.[6], who, using luminescence and absorption procedures, were able to carry out the analysis only at low temperatures (from 4.2 to ~200°K). As seen from Fig. 1, which shows the spectra of the polarized luminescence of $LaF_3:Nd^{3+}$ at 77 and 300°K, connected with the $^4F_{3/2} \rightarrow {}^4I_{11/2}$ transitions, it is impossible to trace the thermal shift of the levels in the region $T > 300$°K, owing to the considerable line broadening.

To solve this problem, we used the method of SE spectroscopy, which enabled us to penetrate into the high-temperature region (up to 820°K for individual lines). The high-temperature lasing experiments, and also experiments using a laser with CAM, enabled us to observe and study SE on seven out of 12 transitions between the $^4F_{3/2}$ and $^4I_{11/2}$ terms. The luminescence spectra ($F_{3/2} \rightarrow I_{11/2}$ transitions) of the combining media used in the CAM lasers to reveal new induced transitions (IT) are also shown in Fig. 1. The level schemes of the $^4F_{3/2}$ and $^4I_{11/2}$ terms in $LaF_3:Nd^{3+}$ are shown for several temperatures in Fig. 2. For convenience in comparing the transitions, the same numbering is used in the figure as for the luminescence spectrum lines (Fig. 1).

The spectroscopic and lasing properties of the $LaF_3:Nd^{3+}$ crystals depend strongly on the mutual orientations of the axes c and F in the investigated samples (Fig. 3). Thus, at 300°K the SE spectrum of the laser with the $LaF_3:Nd^{3+}$ crystal with angle

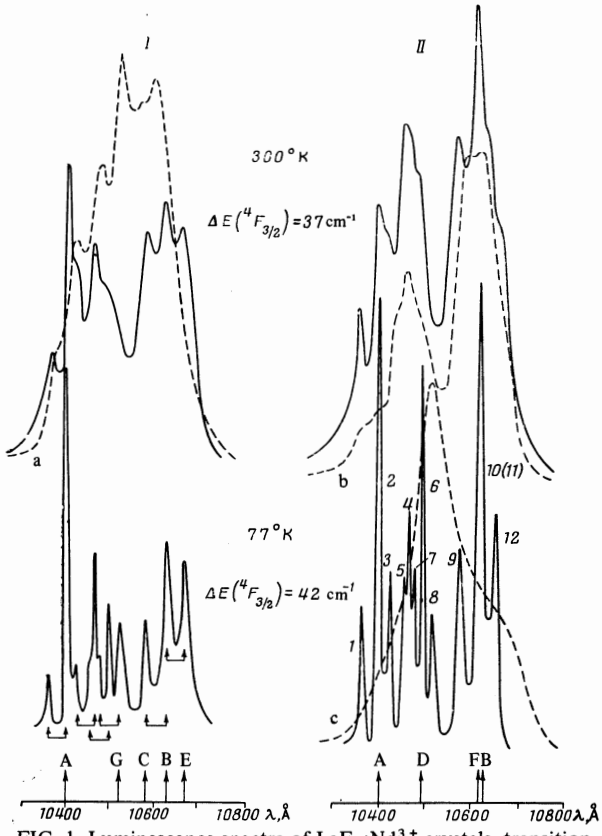

FIG. 1. Luminescence spectra of $LaF_3:Nd^{3+}$ crystals, transition $^4F_{3/2} \rightarrow {}^4I_{11/2}$: I) $\zeta = 20 \pm 3°$, II) $\zeta = 73 \pm 3°$. The square brackets denote the splitting of the term $^4F_{3/2}$. The dashed lines show the luminescence spectra at 300°K of the crystals α-$NaCaYF_6:Nd^{3+}$ (a) and $NaCaCeF_6:Nd^{3+}$ (b) and that of LGS-41K neodymium glass (c), which were used as combined media in lasers with CAM.

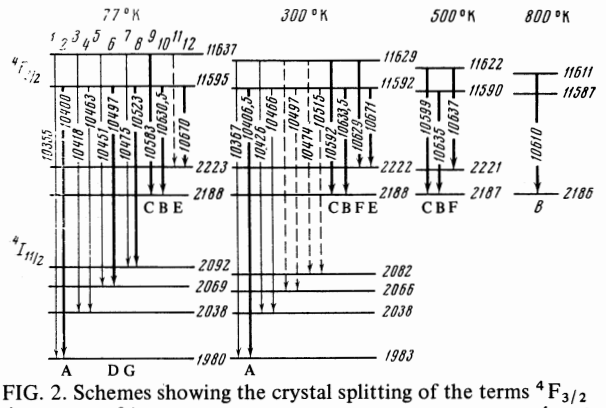

FIG. 2. Schemes showing the crystal splitting of the terms $^4F_{3/2}$ and $^4I_{11/2}$ of Nd^{3+} ions in LaF_3. The levels are indicated in cm^{-1} and the transitions between them in Å. The thin dashed arrows correspond to insufficiently distinct lines in the spectrum, while the thick arrows denote stimulated transitions.

$\zeta \approx 20°$ consists of two lines, A (10 406.5 Å), connected with the transitions 11 592 cm^{-1} $^4F_{3/2} \rightarrow {}^4I_{11/2}$ and 1983 cm^{-1} and 11 592 cm^{-1} $^4F_{3/2} \rightarrow {}^4I_{11/2}$ 2188 cm^{-1} (Fig. 3, spectrum 1). On the other hand, a laser with a crystal having $\zeta = 73°$ generates only on the line B (Fig. 3, spectrum 15). We had at our disposal an $LaF_3:Nd^{3+}$ crystal ($l \approx 7$ mm) with an angle ζ close to zero. A laser on its basis, as seen from the same figure (spectra 12 and 13) generates only on the line A at both 77 and 300°K. At 77°K a laser based on $LaF_3:Nd^{3+}$ emits, in addition to the lines A and B, also on the IT wave D (~10 497 Å), which connects the levels 11 595 cm^{-1} $^4F_{3/2} \rightarrow {}^4I_{11/2}$ 2069 cm^{-1} (Fig. 3, spectrum 14). The considerable broadening of the SE line of the crystal with angle $\zeta \approx 73°$ at T = 500–700°K (spectra 18–20) is apparently connected with the "inclusion" of the transition F, 11 622 cm^{-1} $^4F_{3/2} \rightarrow {}^4I_{11/2}$ 2221 cm^{-1} in the generation (see Fig. 2). The data on the thermal line shift (Fig. 3, spectra 14–20) show that when the temperature is increased the line B shifts towards longer wavelengths with $\Delta\lambda/\Delta T \approx 1.5 \times 10^{-2}$ cm^{-1} deg^{-1}, whereas the line F shifts with $\Delta\lambda/\Delta T \approx 3 \times 10^{-2}$ cm^{-1} deg^{-1}. For T = 500–700°K the generation wavelengths λ_g of these lines almost coincide. The line F could also be "revealed" in experiments with CAM lasers (Fig. 3, spectrum 22). The use of this method also made it possible to register other generation lines. Thus, with CAM on the basis of α-$NaCaYF_6:Nd^{3+}$ (300°K) in an $LaF_3:Nd^{3+}$ crystal ($\zeta \approx 20°$, 300°K) we registered the induced transition C with λ_g = 10 592 Å (spectrum 10), which is excited in the ordinary laser scheme only at T = 360°K (spectrum 2), as well as the transition E (λ_g = 10 670 Å at 77°K and 10 671 Å at 300°K, spectra 10 and 11). When the $LaF_3:Nd^{3+}$ crystal ($\zeta \approx 73°$, T = 77°K) is combined with phosphate glass LGS-41K, the spectrum of the CAM laser contains already four SE lines: G with λ_g = 10 523 Å, C (10 583 Å), B (10 630.5 Å) and E (10 670 Å, spectrum 24). The data on the threshold excitation energies (E_{thr}) for different IT in the $LaF_3:Nd^{3+}$ crystals are given in Table I.

Figure 4 shows the experimental plots of $E_{thr}(T)$ for $LaF_3:Nd^{3+}$ crystals with different orientations. These data supplement the information of Fig. 3 on the temperature dependence of IT. To analyse the

manifestations of the electron-phonon interaction with $LaF_3:Nd^{3+}$, we used the procedures described in[4]. In this connection, we obtained the generation energy E_g as a function of the temperature and of the coefficient $n = E_{exc}/E_{thr}$ (Figs. 5 and 6).

INTERPRETATION OF $E_{thr}(T)$ AND $E_g(n, T)$ PLOTS

We shall analyze theoretically the experimental $E_{thr}(T)$ and $E_g(n, t)$ plots by solving the system of kinetic equations under the following simplifying assumptions. The relaxation between the terms participating in the excitation of the SE is very rapid, there

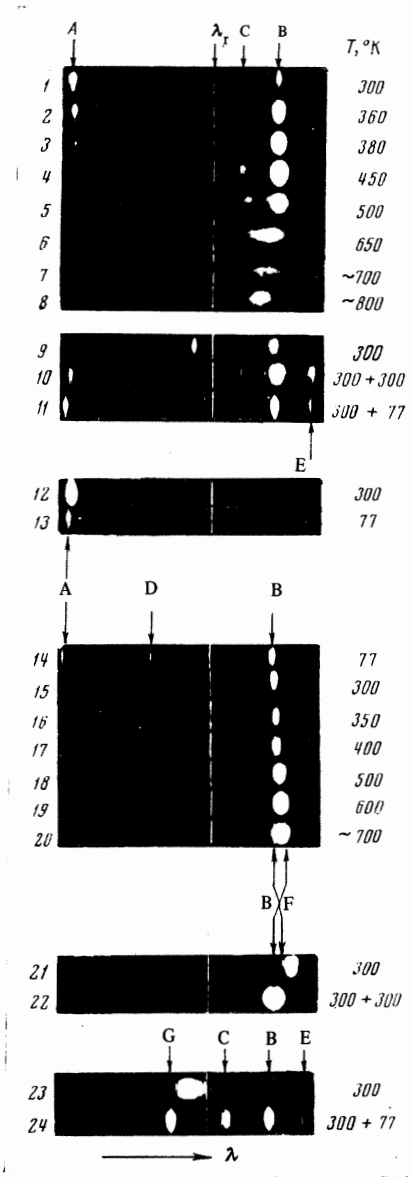

FIG. 3. Stimulated-emission spectra of lasers and CAM lasers based on $LaF_3:Nd^{3+}$ crystals. The reference line is $\lambda_r = 10\,561.5$Å. Number of spectrum, Type of laser, 1-8: Laser with LaF_3-Nd^{3+} ($\zeta \approx 20°$), 9: Laser with α-$NaCaYF_6$-Nd^{3+}, 10-11: CAM laser with α-$NaCaYF_6$-Nd^{3+} + LaF_3-Nd^{3+} ($\zeta \approx 20°$), 12-13: Laser with LaF_3-Nd^{3+} ($\zeta \approx 0°$), 14-20: Laser with LaF_3-Nd^{3+} ($\zeta \approx 73°$), 21: Laser with α-$NaCaCeF_6$-Nd^{3+}, 22: Laser with α-$NaCaCeF_6$-Nd^{3+} + LaF_3-Nd^{3+} ($\zeta \approx 73°$), 23: Laser with LGS-41K, 24: CAM Laser with LGS-41K + LaF_3-Nd^{3+} ($\zeta \approx 73°$).

Table I. Values of E_{thr} for different IT in the $LaF_3:Nd^{3+}$ crystal

Wavelength, Å	SE lines	E_{thr}, J: Laser	Laser with CAM*:		
		LaF_3 — Nd^{3+} **	α-$NaCaYF_6$—Nd^{3+} ***	LGS-41K ****	α-$NaCaCeF_6$—Nd^{3+} ***
		$T = 77°$ K			
10400	A	15	15	—	—
10497	D	20	—	—	—
10523	G	—	—	8	—
10583	C	—	—	15	—
10630,5	B	3	5	5	—
10670	E	—	~100	~150	—
		$T = 300°$ K			
10406.5	A	5	20	—	—
10592	C	—	~50	—	—
10629	F	—	—	—	~25
10633.5	B	20	10	—	~25
10671	E	—	15	—	—

*The temperature of the combining media was 300°K.

**The data are given for lasers with $LaF_3:Nd^{3+}$ ($\zeta \approx 20°$) at 77°K and with $LaF_3:Nd^{3+}$ ($\zeta \approx 73°$) at 300°K.

***The $LaF_3:Nd^{3+}$ ($\zeta \approx 73°$) crystal was used.

****The $LaF_3:Nd^{3+}$ ($\zeta \approx 20°$) crystal was used.

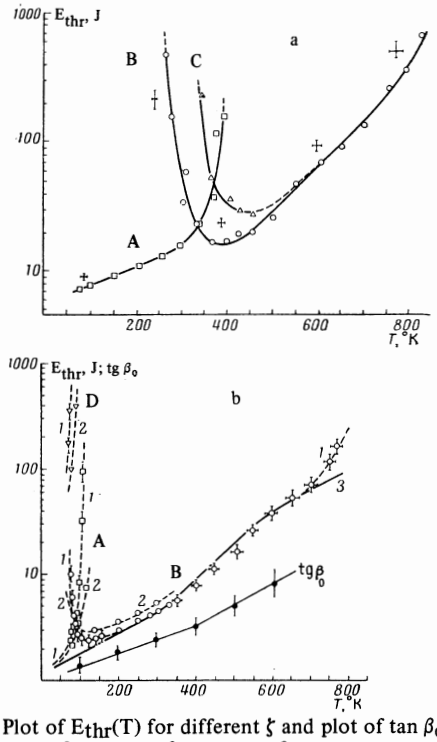

FIG. 4. Plot of $E_{thr}(T)$ for different ζ and plot of tan $\beta_0(T)$ for $\zeta \approx 73°$: a) $\zeta \approx 20°$, b) $\zeta \approx 73°$ (1) and 63° (2); curve 3—theoretical $E_{thr}(T)$ dependence.

are no luminescent $^4F_{3/2} \rightarrow {}^4I_{13/2,15/2}$ transitions (their actual share in the luminescence amounts to about 10%), there is no nonradiative relaxation from the $^4F_{3/2}$ term, and the establishment of temperature equilibrium between the Stark levels of the same multiplet is much faster than between multiplets.

The kinetic equations take the form

$$b_1^x \dot{N}_1 = -b_1^x N_1 (W_{exc} + w_{12}) + N_2 b_2^x w_{21} + N_3 b_3^x A_3^x (1 - \gamma) + N_4 b_4^x A_4^x,$$

$$b_2^x \dot{N}_2 = b_1^x N_1 w_{12} - N_2 \left(b_2^x w_{21} + \sum_x B_x u_x b_x' \right)$$

$$+N_3\left(b_3^{\Sigma}A_3^{x}\gamma+\sum_x B_x u_x b_x\right),$$

$$b_4^{\Sigma}\dot{N}_4=b_1^{\Sigma}N_1W_{exc}+b_3^{\Sigma}N_3w_{34}-b_4^{\Sigma}N_4w_{43}/\eta,\qquad(1)$$
$$N_0=b_1^{\Sigma}N_1+b_2^{\Sigma}N_2+b_3^{\Sigma}N_3+b_4^{\Sigma}N_4,$$
$$\dot{u}_x=-\alpha u_x+B_x u_x h\nu_g(\Delta N)_x,$$

where x is the index of the SE line or of the corresponding transition, the summation being carried out over all transitions on which the SE takes place; W_{exc} is the excitation rate; u_x is the volume radiation density at the frequency of the line x; N_0 is the number of impurity ions per cm^2; α is the loss in the system; A_x and B_x are the Einstein coefficients for the line x; b_i^{Σ} is the sum of the Boltzmann factors of all the Stark levels of the i-th multiplet relative to its lowest component; N_i is the population of this component; i = 1 for $^4I_{9/2}$, i = 2 for $^4I_{11/2}$, i = 3 for $^4F_{3/2}$, and i = 4 for $^4F_{5/2}$; b_x and b'_x are the Boltzmann factors for the initial and final levels of the transition x; γ is the fraction of luminescence belonging to the transitions $^4F_{3/2}\rightarrow{}^4I_{11/2}$;

$$A_i^{x}=\frac{1}{b_i^{x}}\sum_x b_x A_x,\quad w_{il}=\frac{1}{b_i^{x}}\sum_x b_x w_x,$$

where the summation is carried out in the first case over all the transitions from the levels of the i-th term to the lower-lying states and in the second case over all the transitions between the terms i and l; w_x is the probability of nonradiative relaxation for the transition x; $\eta=w_{43}/(w_{43}+A_4^{\Sigma})$.

Solving the system in the stationary approximation and assuming that $w_{43}\gg w_{21}>A_3^{\Sigma}$, we obtain

$$u_x=C_x\frac{\eta W_{exc}-\eta W_{exc}^{thr}}{F_x\eta W_{exc}+1},\qquad(2)$$

where

$$\eta W_{exc}^{thr}=\frac{b_3^{x}A_3^{x}}{\delta_x-b_3^{x}}\left(1+\frac{\delta_x}{b_1^{x}}y\right)\left(1+\eta\frac{b_4^{x}A_4^{x}}{b_3^{x}A_3^{x}}z\right)\qquad(2a)$$

$$\delta_x=\frac{N_0h\nu_g}{\alpha}B_xb_x=\frac{N_0}{\alpha}\left(\frac{v_0}{2\pi\nu_g}\right)^2\frac{b_xA_x}{\Delta\nu_{lum}^{x}}\qquad(2b)$$

$$F_x=\left(1+\frac{b_x'b_3^{x}}{b_xb_2^{x}}\right)\frac{1}{w_{21}},\quad C_x=\frac{\delta_x-b_3^{x}}{B_xb_x}.\qquad(2c)$$

Here ηW_{exc}^{thr} is the threshold value of the excitation rate, $y=N_2/N_{1\gamma}$ $z=N_4/N_3$, v_0 is the velocity of light in the crystal, and $\Delta\nu_{lum}^{x}$ is the width of the luminescence line x. In the case of resonance, i.e., when several transitions take part in the SE at the frequency ν_g, it is necessary to substitute in (2a) and (2b) a value of δ_{eff} equal to the sum δ_x of the corresponding lines.

Assuming that $E_{exc}\sim\eta W_{exc}$ at all values of T and n (and $E_{thr}\sim\eta W_{exc}$) and that $\delta_x\gg b_3^{\Sigma}$, we can introduce into formula (2) the coefficient n and transform this formula into

$$E_g(n)=\operatorname{tg}\beta_0\frac{n-1}{1+na_0},\qquad(3)$$
$$\operatorname{tg}\beta_0=k_0t_g\eta W_{exc}^{thr},\quad a_0=\eta W_{exc}^{thr}F_x,$$

where $k_0=N_0Vh\nu_{3K}$ is a coefficient independent of the temperature, K is the ratio of the output loss to the total loss in the system, t_g is the duration of the SE, and V is the volume of the crystal. We shall henceforth assume that K and t_g are independent of n. At $na_0\ll 1$ formula (3) is transformed into the well known formula $E_g(n)$ (see[7], Vol. 1, Sec. 11).

From (2) we can also readily obtain an expression for the laser efficiency:

$$f=k_0t_g\frac{n-1}{n}\frac{1}{1+s(\eta W_{exc}/w_{21})}\qquad(4)$$

The coefficient s replaces the factor $(1+b_x'b_3^{\Sigma}/b_xb_2^{\Sigma})$, which depends weakly on the temperature.

To calculate E_{thr} by formula (2) it is necessary to know the probabilities A_x of the transitions between the Stark levels of the states $^4F_{3/2}$ and $^4I_{11/2}$. In uniaxial crystals such as LaF_3, these data can be gotten from the luminescence spectra obtained for two different orientations. The probability A_x is given by the formula

$$A_x=\gamma A_3^{x}\beta_x(T)(b_3^{x}/b_x),$$

where

$$\beta_x(T)=\beta_x'(T,\zeta)/\Phi_x(\zeta),$$

$\beta_x'(T,\zeta)$ is the spectral density of the luminescence

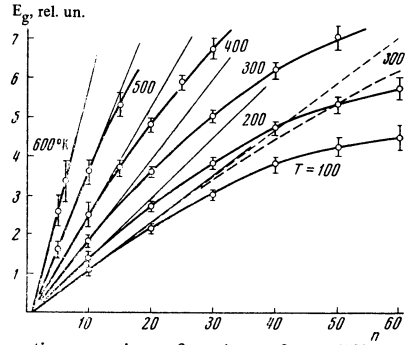

FIG. 5. Generation energies as functions of n at different temperatures (marked on the curves) for $LaF_3:Nd^{3+}$ crystals (continuous curves) and for a $Y_3Al_5O_{12}:Nd^{3+}$ crystal (dashed).

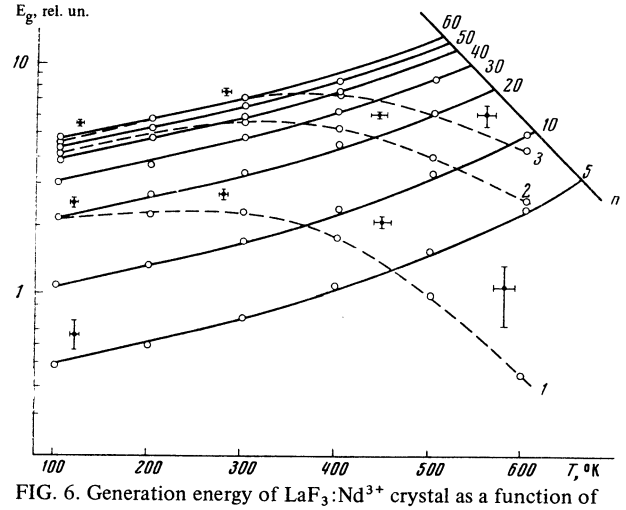

FIG. 6. Generation energy of $LaF_3:Nd^{3+}$ crystal as a function of the temperature at different values of n (continuous curves) and at different excitation powers: 1) $E_{exc}\sim 80$ kW, 2) $E_{exc}\sim 180$ kW; 3) $E_{exc}\sim 300$ kW.

for the line x in the case of observation at an angle ζ to the optical axis of the crystal; $\Phi_x(\zeta)$ is a function that determines the dependence of the line intensity x on the direction.

The forms of the functions $\Phi_x(\zeta)$ for crystals having different symmetries are given in[8]. In a uniaxial crystal with symmetry axis C_6 when the luminescence is excited with unpolarized light, we have

$$\Phi_x(\zeta) = {}^3/_2[{}^1/_2 \sin^2\theta_x(1+\cos^2\zeta) + \cos^2\theta_x \sin^2\zeta],$$

where θ_x is a parameter determined from experiment. Using the luminescence spectra (Fig. 1) and the values $A_3 = 1430\ \text{sec}^{-1}$ and $\gamma = 0.68$, we have determined the values of A_x, θ_x, and $\beta_x(77^\circ\text{K})$ for most transitions between the terms $^4F_{3/2}$ and $^4I_{11/2}$ (Table II).

To verify the obtained values of A_x and θ_x, we calculated the locus of the points of equality of the generation thresholds for the lines A and B in terms of the coordinates T and ζ (Fig. 7). The accuracy with which the quantities A_A, A_B, and A_F are known turned out to be insufficient for a reliable determination of the theoretical curve at $\zeta = 0^\circ$. At $T < 400$–500°K, when we have $y, z \ll 1$ and $\delta_x \gg b_3^\Sigma$ in (2a), the thresholds for the lines A and B become equal to each other if $\delta_A = \delta_B$. As seen from Table II, the difference between the absolute values of A_A and A_B and between their angular dependences is small. At the same time, the widths of these lines differ noticeably at $T \lesssim 500^\circ$K (see below), so that E_{thr} for these lines can be equal only at high temperatures. This contradicts the experimental data for $\zeta \approx 73^\circ$ (Fig. 4b). To reconcile the calculations it was recognized that the line B overlaps to a considerable degree the line E, and consequently the condition for the equality of the thresholds is $\delta_A = \delta_{eff}$. The line F is connected with the upper component of the term $^4F_{3/2}$, and its intensity increases with temperature. As a result, the gain at the frequency of the line B also increases with the temperature, and E_{thr} for this line becomes lower than the generation threshold of line A. The shift of the point of equality of E_{thr} with changing orientation of the crystal is due to the fact that the line F has an angular dependence of intensity much different from those of the lines A and B.

With the aid of the quantities A_x and the experimental data on $\Delta\nu_{lum}^A$ and $\Delta\nu_{lum}^B$ (Fig. 8), we used formula (2) to calculate the relative change of $E_{thr}(T)$ for the crystal with $\zeta \approx 73^\circ$ (Fig. 4b). These calculations have shown that up to $T = 300^\circ$K the predominant factor determining the temperature dependence of E_{thr} is the change of the line width. At higher values of T, the lowering of the pumping efficiency, due to the relaxation transitions $^4F_{3/2} \rightarrow {}^4F_{5/2}$, comes into play. At $T = 400^\circ$K, this factor increases the threshold by about 30%. The best agreement with experiment was obtained at $\eta A_4^\Sigma / A_3^\Sigma = 2.5$. For an exact description of the $E_{thr}(T)$ dependence at $T > 500^\circ$K, it is also necessary to take into account the Boltzmann population of the $^4I_{11/2}$ state. This factor accounts for about 15% of E_{thr} already at $T = 500^\circ$K. The sharp increase of E_{thr} at temperatures above 700°K is determined by factors that are not accounted for in the assumed model.

The high-temperature investigations of SE in a large number of crystals activated with Nd^{3+} ions have shown that their $E_{thr}(T)$ dependences are different up to $T = 400^\circ$K, and are approximately the same in the interval $T = 400$–700°K (see Figs. 3 and 7 of[3]). The reason for this is as follows. Up to $T \approx 400^\circ$K, the change of $E_{thr}(T)$ is determined by the change $\Delta\nu_{lum}$, which is different in its character for all the crystals. At higher temperatures, the form of the $E_{thr}(T)$ curve begins to depend in significant fashion on the energy gaps between the terms $^4I_{11/2}$ and $^4I_{9/2}$ and between $^4F_{3/2}$ and $^4F_{5/2}$. These gaps vary little from crystal to crystal, and this results in the same dependence of E_{thr}.

Figure 5 shows plots of $E_g(n)$ obtained at different temperatures. The same experimental results are plotted in terms of different coordinates in Fig. 6. It is seen from these figures that E_g increases with temperature at a constant value of n. At small n, this is due to the increase of ηW_{exc}^{thr} with increasing temperature (the approximate correspondence between the tan $\beta_0(T)$ and $E_{thr}(T)$ plots shown in Fig. 4b indicates

Table II

Line*	θ_x, deg	β_x (77°)	A_x, sec^{-1}	Line*	θ_x, deg	β_x (77°)	A_x, sec^{-1}
1	45	0.046	140	6 (D)	45	0.085	120
2 (A)	65	0.124	180	8 (G)	80	0.071	100
3	40	0.053	165	9 (C)	55	0.110	340
4	—	0.152	(160)	10 (B)	70	0.140	195
5	—		(100)	11 (F)	~0	0.084	260
7	—			12 (E)	80	0.135	190

*The lines are numbered in accordance with Figs. 1 and 2.

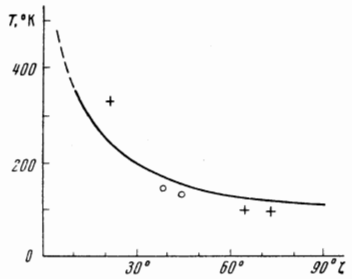

FIG. 7. Angular and temperature dependences of the point of equality of E_{thr} of the lines A and B in a laser based on $LaF_3:Nd^{3+}$. The continuous line is the result of the calculation, and the circles mark the experimental data obtained in [9] (according to our data, the angle between c and F in [9] is equal to $90^\circ - \zeta$).

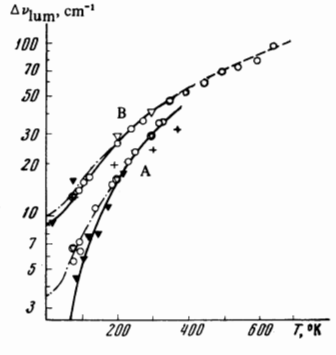

FIG. 8. Comparison of experimental and theoretical (continuous line) temperature broadening of the lines A and B of a laser based on $LaF_3:Nd^{3+}$. Luminescence data: ▽–present work, ▼–[6], +–[10], ○–generation data.

that under our excitation conditions t_g varies little with the temperature). With increasing n, saturation of the output energy sets in. At $na_0 \gg 1$, the output energy approaches, in accordance with (3), a constant value $E_g^{sat} = k_0 t_g w_{21}/s$, the temperature dependence of which is due to the acceleration of the nonradiative relaxation from the term $^4I_{11/2}$. As shown by the data of Fig. 5, in the experiment at $T \leq 500°K$ it was possible to obtain values of n such that the effect of saturation of E_g is already quite clearly pronounced and can be used to estimate the relative variation of w_{21} with changing temperature.

According to (4), the effectiveness f(T) at a constant excitation rate should be different and depend on the ratio of ηW_{exc} and w_{21}. If $\eta W_{exc} \ll w_{21}$ (T = 0), then f decreases with temperature, since n decreases. On the other hand, if $\eta W_{exc} > w_{21}$ (T = 0), then f increases in a certain temperature interval before it begins to decrease as a result of the decrease of n. Thus, the f(T) curve will have a maximum. With increasing ηW_{exc}, the maximum point should shift towards higher temperatures. The height of the maximum then increases, since the $w_{21}(T)$ dependence becomes steeper with increasing temperature. All this is seen in Fig. 6.

BROADENING AND SHIFT OF LINES

Investigations of the shift and broadening of the luminescence lines are carried out, as a rule, to temperatures smaller by a factor 1.5–2 than the Debye temperature Θ_D; at these temperatures, $\Delta\nu_{lum}$ does not exceed the Stark splitting. In experiments on SE, with crystals activated by Nd^{3+} ions, the range of these investigations can be extended. Such a possibility exists if the spectral lines adjacent to the generation line actually differ from the latter in intensity or in polarization properties. Then the contribution of these lines to the SE can be neglected even if they overlap appreciably, and it can be assumed that the position of the generation lines corresponds to the maximum of the luminescence line. The width of the luminescence line at high temperatures can be estimated from the value of $\Delta\nu_g$. In media with homogeneous line broadening, $\Delta\nu_g$ is determined by the spontaneous emission in the high-Q modes, and at constant values of n it varies in proportion to $\Delta\nu_{lum}$[11]. This was verified by us for a number of crystals[4], including $LaF_3:Nd^{3+}$.

The positions and widths of the lines in the LaF_3 crystals were investigated for the ions Pr^{3+} [12] and Nd^{3+} [6]. The line shift in[6] was traced up to ~150°K, and the broadening to ~200°K. In SE experiments up to temperatures higher than in[6], we succeeded in measuring the broadening of the lines A and B and the shifts of the lines A, B, and C. These data are shown in Figs. 8 and 9, respectively. The values of $\Delta\nu_g$ were plotted in such a way as to make them coincide with the values of $\Delta\nu_{lum}$ at low temperatures.

The theory of the temperature behavior of the width and position of the spectral lines in impurity crystals was developed in[13], where the contribution of the phonons with large wave vector was neglected, and a Debye shape of the spectrum was assumed for the long-wave phonons. Investigations performed on a number of crystals[4,13-15] have shown that the formulas obtained

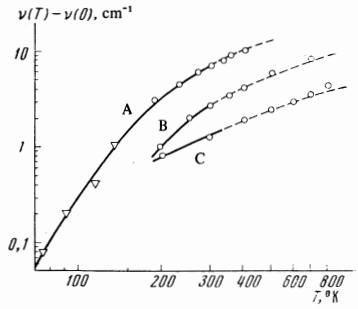

FIG. 9. Comparison of experimental and theoretical (continuous lines) plots of the temperature shift of the generation lines of a laser based on $LaF_3:Nd^{3+}$: ▽–luminescence data [6]; ○–generation data. For line C, the absolute value of $\nu(T)-\nu(0)$ has been decreased by a factor of 5.

in[13] give the correct course of the broadening and of the shift of the lines with temperature, but necessitate the introduction of a certain effective value of the Debye temperature, $T_D < \Theta_D$. Using $MgO:Cr^{3+}$ as an example, it was shown in[16] that when all the crystal vibrations interacting with the impurity ion are taken into account, good agreement with experiment is obtained at $T_D = \Theta_D$. Better agreement is also obtained by using in the calculation the real form of the impurity-active phonon spectrum, obtained from the electron-vibrational structure[15].

In the interpretation of the experimental data, we have used the formulas of[14], expressed in the following form:

$$\Delta\nu_{lum}^{x}(T) = \sum \beta_{br}\left(\frac{\nu}{c}\right)\bar{n}\left(\frac{\nu}{c}\right) + \sum \beta_{br}\left(\frac{\nu}{c}\right)\left[\bar{n}\left(\frac{\nu}{c}\right)+1\right] + \bar{\alpha}_1(x)\xi_6\left(\frac{T_D}{T}\right),$$

$$\nu_x(T) - \nu_x(0) = \sum \beta_{sh}\left(\frac{\nu}{c}\right)\xi\left(\frac{\nu}{c}\right) + \alpha_1(x)\xi_3\left(\frac{T_D}{T}\right), \qquad (5)$$

where $\bar{n}(\nu/c)$ is the occupation number of the phonons with energy ν/c; the summation is carried out over all the direct relaxation transitions that contribute to the broadening and shift of the line x. In (5), the coefficients β_{br} and β_{sh} characterize the broadening and shift of the individual energy levels, due to direct transitions between the levels x_i and x_j, the energy of which is indicated in the parentheses:

$$\beta_{sh}\left(\frac{\nu}{c}\right) = (E_{x_j} - E_{x_i})\,|\langle x_j|C|x_i\rangle|^2 \frac{(kT_D)^2}{2\pi^2\rho v^5\hbar^3} \qquad (6)$$

$$\beta_{br}\left(\frac{\nu}{c}\right) = \pi\left(\frac{h\nu}{kT_D}\right)^2 \left|\beta_{sh}\left(\frac{\nu}{c}\right)\right|^2. \qquad (7)$$

The contribution of the Raman processes to the broadening and shift of the level x_i is characterized by the coefficients

$$\bar{\alpha}_1(x_i) = \frac{\bar{a}(kT_D)^7}{2\pi^3\rho^2\hbar^6 v^{10}}, \quad \alpha_1(x_i) = \frac{a(kT_D)^4}{2\pi^2\rho\hbar^3 v^5} \qquad (8)$$

The same coefficients for the line x are

$$\bar{\alpha}_1(x) = \bar{\alpha}_1(x_i) + \bar{\alpha}_1(x_j), \quad \alpha_1(x) = \alpha_1(x_i) - \alpha_1(x_j). \qquad (9)$$

In addition, we have introduced in (5) the notation

$$\xi_5(z)=\frac{1}{z^4}\int_0^z \frac{x^3}{e^x-1}dx, \quad \xi_6(z)=\frac{1}{z^7}\int_0^z \frac{x^6e^x}{(e^x-1)^2}dx,$$

$$\xi\left(\frac{\nu}{c}\right)=\frac{1}{z^2}\int_0^z \frac{x^3}{e^x-1}\frac{1}{x^2-(h\nu_{ij}/kT)^2}dx,$$

where $\xi(\nu/c)$ is the principal value of the integral; $\bar{a}$ and a are coefficients containing the matrix elements of the operators C and D, which characterize the electron-phonon interaction components that are linear and quadratic in the lattice vibrations[12,14], and v is the averaged velocity of sound.

The dash-dot curves in Fig. 8 give the temperature dependence of the line width with allowance for the inhomogeneous broadening. The curves were calculated under the assumption that this broadening is the same for both lines and equals $\sim 3.5\ cm^{-1}$. The addition of the homogeneous and inhomogeneous parts of the line width was carried out with the aid of Posener's table[17].

Formulas (5) are valid, strictly speaking, only for $T \ll \Theta_D$. However, the results of our calculations in accordance with these formulas also agree well with the experimental points in the region $T \geq T_D$[1] (see Figs. 8 and 9, where they are shown dashed). This can be attributed to the fact that we used in the calculation the value $T_D = 360°K$, determined in[12] from the form of the electron-vibrational spectrum of the Pr^{3+} ions in LaF_3. This method is equivalent to taking into account the real form of the spectrum of the impurity-active phonons, and apparently weakens somewhat the limitations imposed on the region of application of the indicated formulas.

Initially[4] the shift of the lines A, B, and C was interpreted as due exclusively to the Raman electron-phonon interaction processes. However, such an approach turned out to be ineffective in the interpretation of the $\Delta\nu_{lum}^{A,B}(T)$ dependences. Allowance for the direct processes $Y_1 \longleftrightarrow Y_2$ ($\Delta E \approx 60\ cm^{-1}$), $Y_5 \longleftrightarrow Y_6$ ($\Delta E \sim 35\ cm^{-1}$), $R_1 \longleftrightarrow R_2$ ($\Delta E \sim 40\ cm^{-1}$), and Y_5, $Y_1 \longleftrightarrow Y_3, Y_4$ ($\Delta E \sim 100\ cm^{-1}$) improved the situation (Y_i and R_i denote here the Stark levels of the terms $^4I_{11/2}$ and $^4F_{3/2}$ in increasing order of energy). The integrals $\xi(40)$, $\xi(60)$, and $\xi(100)$ were calculated for $T = 10$–$1000°K$. At $T > 40°K$, these integrals are positive and the direct processes corresponding to them lead to a "coming together" of the levels. From the coefficients in (5), the values of $\beta_{br}(60)$ and $\beta_{br}^{Y_5 \longleftrightarrow Y_3,Y_4}(100)$ were estimated from the value of the homogeneous broadening of the lines $R_1 \longleftrightarrow Y_2$, Y_5 at $T = 0$. In the calculations, we assumed for them the values 0.5 and 8.8 cm^{-1}, which are close to those obtained in[6]. The remaining coefficients in $\Delta\nu_{lum}^{A,B}(T)$ were selected to fit. The best agreement between the theoretical and experimental plots of $\Delta\nu_{lum}^{A,B}(T)$ was obtained at the following values:

$$\beta_{br}(35)=0.2\ cm^{-1},\ \beta_{br}(40)=2.3\ cm^{-1},\ \beta_{br}^{Y_1 \longleftrightarrow Y_3,Y_4}(100)=3\ cm^{-1},$$
$$\bar{a}_1(A)=95\ cm^{-1},\ \bar{a}_1(B)=37\ cm^{-1}.$$

The coefficients β_{sh} were determined from the values of the corresponding β_{br} with the aid of (7):

$$\beta_{sh}(35)=3{,}2\ cm^{-1},\ \beta_{sh}(40)=28\ cm^{-1},\ \beta_{sh}(60)=3\ cm^{-1},$$
$$\beta_{sh}^{Y_1 \longleftrightarrow Y_3,Y_4}(100)=6\ cm^{-1},\ \beta_{sh}^{Y_5 \longleftrightarrow Y_3,Y_4}(100)=17.5\ cm^{-1}.$$

After substituting these quantities in (5), we obtain the coefficients α_1:

$$\alpha_1(A)=-110\,cm^{-1},\ \alpha_1(B)=-140\ cm^{-1},\ \alpha_1(C)=+13.6\,cm^{-1}.$$

According to (6) and (7), $\beta_{br}(\nu/c) \sim \nu^3$. In contrast, the values of $\beta_{br}(\nu/c)$ obtained above reveal no definite frequency dependence. This is undoubtedly due to a considerable degree to the fact that the calculations took no account of the contributions of a large number of direct relaxation transitions between the levels, so that the obtained coefficients $\beta_{br}(\nu/c)$ are effective quantities. Nonetheless, the values of $\beta_{sh}(\nu/c)$ obtained from $\beta_{br}(\nu/c)$ account qualitatively quite well for the shifts obtained by Johnson et al. (see Fig. 4 in[6]) for the $^4I_{11/2}$ levels at $T < 200°K$. Thus, the almost parallel decrease of the energies of the levels Y_5 and Y_6 agrees with the small value of $\beta_{sh}(35)$ and with the large value of $\beta_{sh}^{Y_5 \longleftrightarrow Y_3,Y_4}(100)$. Our values of $\beta_{sh}(\nu/c)$ do not explain the minimum in the $E_{Y_1}(T)$ dependence. It is possible that it is due to the influence of the induced phonon transitions $Y_1 \longleftrightarrow Y_5$, Y_6 ($\Delta E \approx 200\ cm^{-1}$). The integral $\xi(200)$ is negative at $T < 300°K$, corresponding precisely to a "repulsion" of the energy levels. By verifying this variant and using the calculated values of $\xi(200)$, we were unable, however, to find a suitable set of coefficients describing satisfactorily the data on $\Delta\nu_{lum}^{A}(T)$.

The mean-squared matrix element $|\langle x_j | C | x_j \rangle|^2$, estimated from the values of β_{br}, is equal to $10^6\ cm^{-2}$ (in the estimate we have assumed $\rho = 6\ g/cm^3$ and $v = 3.44 \times 10^5\ cm/sec$[18]). Measurements of the rate of spin-lattice relaxation in $LaF_3:Nd^{3+}$ give for the same quantity a value $1.2 \times 10^5\ cm^{-2}$[18]. According to our data, $|\langle R_2 | C | R_1 \rangle|^2 = 4.5 \times 10^6\ cm^{-2}$. This corresponds to a nonradiative relaxation rate of $7 \times 10^{11}\ sec^{-1}$ between the components of the $^4F_{3/2}$ term.

TEMPERATURE DEPENDENCE OF w_{21}

In several of the presently known investigations[19,20] the magnitude and the temperature dependence of the NT probabilities were determined from the temperature quenching of the luminescence. The use of this method is limited to transitions where the nonradiative channel is significant as well as the nonradiative one. Information on the rate of deactivation of the levels

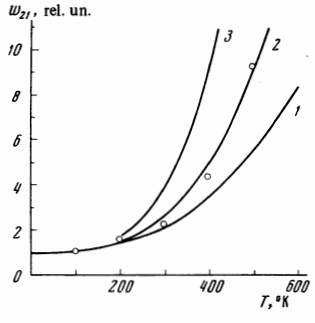

FIG. 10. Temperature dependence of the probability w_{21}. The theoretical curves 1, 2, and 3 have been calculated for four-, five-, and six- phonon relaxation processes, respectively.

[1] The value of Θ_D for LaF_3 is unknown.

with predominantly nonradiative decay can be obtained in experiments on luminescence excitation[19] or in lasing experiments[21] with the luminescence or SE excited with the aid of lasers operating in the giant-pulse regime. The accuracy with which the NT probabilities are estimated by these methods is insufficient for the investigation of its temperature dependence. For such levels, this dependence can be determined by the method proposed in[4].

From the expression for a_0 (see (3)) we obtain the following formula, which is convenient for the determination of $w_{21}(T)$:

$$w_{21} = s\eta W_{\text{exc}}^{\text{thr}} / a_0. \tag{10}$$

For calculations with the aid of this formula, the relative change of $\eta W_{\text{exc}}^{\text{thr}}$ with temperature is obtained from experiment (Fig. 4), and the value of a_0 is determined from the data of Fig. 5 with the aid of the relation

$$\frac{E_g(n)}{E_g(n')} = \frac{n-1}{n'-1}\frac{1}{1+(n-n')a_0},$$

where $n'a_0 \ll 1$ and n' is a fixed value of n. In the case of $LaF_3:Nd^{3+}$, this parameter is independent of n or T within the limits of the possible error.

The $w_{21}(T)$ dependence was calculated using a simplified model of a relaxational transition, according to which it is realized with the aid of the emission of m phonons with identical energy $h\nu_{ph}$:

$$w_{21}(T) = w_{21}(0)\,[\bar{n}(h\nu_{ph}) + 1]^m. \tag{11}$$

The results of calculations by means of formulas (10) and (11) are shown in Fig. 10. Curve 3 on this figure was obtained under the assumption that the NT proceed from the lowest level of the $^4I_{11/2}$ term to the upper component of the ground state, m = 6, and curve 2 was obtained under the assumption that the relaxation proceeds from the two lower levels of the term $^4I_{11/2}$, m = 5. In both cases, the change in the particle distribution among the $^4I_{11/2}$ levels with changing temperature was taken into account. Curve 1 on Fig. 10 was obtained under the assumption that the relaxation proceeds with identical probability from all the components of $^4I_{11/2}$, m = 4. We see that the experimental $w_{21}(T)$ plot corresponds to a five-quantum process realized by emission of phonons with $h\nu_{ph} = 295\ cm^{-1}$.

Actually, the relaxation proceeds via a number of partial channels corresponding to emission of different combinations of phonons. Therefore the quantity $h\nu_{ph}$ determined from the comparison of the theoretical and experimental $w_{21}(T)$ dependences is an effective quantity, which, generally speaking, may not correspond to any real lattice vibration. In the case of LaF_3, however, an investigation of the Raman scattering[22] has revealed intense lattice oscillations with phonon energies 290 and 315 cm^{-1}, which are very close to the obtained value of $h\nu_{ph}$. These oscillations take an active part in the electron-phonon interactions with the impurity ions that replace the La, as indicated by the presence of corresponding maxima in the impurity-active phonon spectrum obtained in[12].

As already noted in[4], the proposed method of determining w_{21} is indirect and one should not expect from it a high accuracy of the absolute value of the probability. Thus, an estimate of w_{21} in accordance with formula (10), using for T = 300°K the values s = 1.3, $\eta W_{\text{exc}}^{\text{thr}}$ = 20--40 sec^{-1} (calculations in accordance with formulas (2a) and (2b) or using the experimental value of $\tan\beta_0$ from formula (3)), and $\alpha_0 = (9 \pm 3) \times 10^{-3}$ yields $w_{21} = 10^3$—10^4 sec^{-1}. The sources of the uncertainties in indicated values of the parameters are the deviations of the real experimental conditions from those assumed in the interpretation of the described $E_g(n, T)$ relations. These deviations include failure to satisfy the conditions of stationary generation, the laser spike regime, and also the influence of the nonoptimal transmission of the output mirror, which possibly exerted an influence at large E_{exc} (see[7], Vol. 1, Sec. 7). The latter circumstance obviously could not cause a temperature dependence of E_g, but it could lead to observation of too low a value of E_g at large n, i.e., increase the parameter a_0. There are therefore grounds for assuming that the volume w_{21} obtained above for $LaF_3:Nd^{3+}$ is somewhat underestimated. We note here also that Fig. 5 shows a plot of $E_g(n)$ at T = 300°K for $Y_3Al_5O_{12}:Nd^{3+}$. This plot has a smaller slope and exhibits saturation at larger n than $E_g(n)$ for $LaF_3:Nd^{3+}$. The corresponding estimates for garnet yield relatively smaller values of $\eta W_{\text{exc}}^{\text{thr}}$ and a_0 than for $LaF_3:Nd^{3+}$, and a larger value of the probability $w_{21} = 10^4$—10^6 sec^{-1}[4], which is in qualitative agreement with the results of a comparison of $E_g(n)$ for both crystals.

In conclusion, we are grateful to Professor Yu. E. Perlin and B. S. Tsukerblat for a fruitful discussion and for a review of the manuscript of the article, to V. F. Miuskov for orienting the crystals, to L. Li for help, and V. V. Osiko, Yu. P. Rudnitskiĭ, and B. P. Sobolev for supplying the active media for the experiments.

[1] A. A. Kaminskii, Opto-Electronics **3**, 19 (1971).
[2] A. A. Kaminskiĭ, Zh. Eksp. Teor. Fiz. **54**, 1659 (1968) [Sov. Phys. JETP **27**, 889 (1968)]; Zh. Eksp. Teor. Fiz., Pis'ma Red. **7**, 260 (1968) [JETP Lett. **7**, 201 (1968)].
[3] A. A. Kaminskiĭ, Zh. Eksp. Teor. Fiz., Pis'ma Red. **6**, 615 (1967) [JETP Lett. **6**, 115 (1967)]; Zh. Eksp. Teor. Fiz. **54**, 727 (1968) [Sov. Phys. JETP **27**, 388 (1968)].
[4] A. A. Kaminskii and D. N. Vylegzhanin, IEEE J. Quantum Electron. **7**, 329 (1971).
[5] A. A. Kaminskiĭ, Zh. Eksp. Teor. Fiz. **56**, 83 (1969) [Sov. Phys. JETP **29**, 46 (1969)].
[6] S. A. Johnson, H. G. Freie, A. L. Schawlow, and W. M. Yen, J. Opt. Soc. Amer. **57**, 734 (1967).
[7] B. I. Stepanov, ed. Metody rascheta opticheskikh kvantovykh generatorov (Methods of Laser Design), Nauka i tekhnika, Minsk, 1966.
[8] K. H. Hellwege, Z. Phys. **121**, 589 (1943).
[9] A. M. Prokhorov, V. A. Sychugov, and G. P. Shipulo, Zh. Eksp. Teor. Fiz. **56**, 1806 (1969) [Sov. Phys. JETP **29**, 970 (1969)].
[10] W. W. Holloway, J. M. Kestigian, F. F. Y. Wang, and G. F. Sullivan, J. Opt. Soc. Amer. **56**, 1409 (1966).
[11] S. G. Odulov, Author's Abstract of Candidate's Dissertation, Physics Institute, Ukrainian Academy of Sciences, Kiev, 1971.
[12] W. M. Yen, W. C. Scott, and A. L. Schawlow, Phys. Rev. A (1964–1965) **136**, 271 (1964).
[13] D. E. McCumber and M. D. Sturge, J. Appl. Phys. **34**, 1682 (1963).
[14] T. Kushida, Phys. Rev. **185**, 500 (1969).
[15] G. F. Imbush, W. M. Yen, A. L. Schawlow, D. E. McCumber, and M. D. Sturge, Phys. Rev. A (1964–1965) **133**, 1029 (1964).
[16] C. Y. Huang, Phys. Lett. A **28**, 461 (1968).

[17]D. W. Posener, Aust. J. Phys. **12,** 184 (1959).
[18]M. B. Schulz and C. D. Jeffries, Phys. Rev. **149,** 270 (1966).
[19]G. M. Zverev, G. Ya. Kolodnyĭ, and A. M. Onishchenko, Zh. Eksp. Teor. Fiz. **60,** 920 (1971) [Sov. Phys. JETP **33,** 497 (1971)].
[20]L. A. Riseberg and H. W. Moos, Phys. Rev. **174,** 429 (1968).
[21]A. A. Zlenko, A. M. Prokhorov, V. A. Sychugov, and G. P. Shipulo, Zh. Eksp. Teor. Fiz. **59,** 785 (1970) [Sov. Phys. JETP **32,** 430 (1971)]; V. A. Sychugov and G. P. Shipulo, Zh. Eksp. Teor. Fiz. **58,** 817 (1970) [Sov. Phys. JETP **31,** 438 (1970)].
[22]R. P. Bauman and S. P. S. Porto, Phys. Rev. **161,** 842 (1967).

Translated by J. G. Adashko
83